Egyptian Journal of Geology

https://egjg.journals.ekb.eg

Elicitation of the tectonic shearing structures in the northeastern part of Sirt Basin, Libya as deduced by potential field data

Hussein T. El-Badrawy, Mostafa Nagy and **Hamed A. Alrefaee**[*]

Geology Department, Faculty of Science, Kafr Elsheikh University, Egypt

THE PRESENT study intends to elicit subsurface shear (wrench) zones that affected the northeastern part of Sirt Basin area, which is considered as one of the most important hydrocarbons-producing regions, and its impact on similar areas around the world. Several techniques have been carried on gravityand magnetic data to achieve this goal, such as least squares, tilt angle derivative, horizontal gradient, and sourceedge detection. In addition, power spectrum and Euler deconvolution methods have been carried out with a view to depict clearly faulting pictures along successive depths of deep-seated structures. 2D modelling has been constructed along two profiles and with the aid of data available from four drilled wells in the study area. New eleven sets of wrench zones that have not been extracted before could be revealed from the interpreted tectonic map and faulting pictures of the study area, mostly of sinistral and dextral strike-slip movements. Also, these zones were traced on six successive levels to know whether they are superficial or deep. Seven sets were revealed from gravity data and six from RTP data. Two sets of shears traced from gravity coincide with two shears from the RTP map. Some of these zones intersect with each other. These intersection points weakened the Earth's crust which in turn becomes tectonically unstable in this area. These wrench zones are predicted to be due to tectonic movements of the Arabian and African plates and additionally the ensuing East African Rift which led the Megashear System of North Africa to reactivate in a dextral strike-slip pattern. Sinistral transtensional reactivationsalong the northwest faults resulted due dextral reactivation of the Megashear System of North Africa.
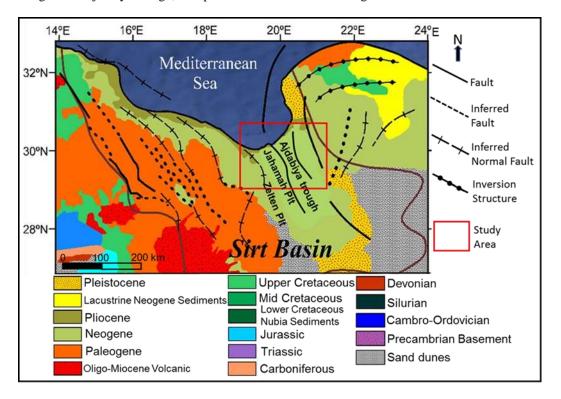
Keywords: Sirt Basin, Libya, gravity and magnetic data, shear zones.

1. Introduction

The Sirt Basin occupies northern central Libya, covering an area of about 500.000 km^2 as shown in Figure (1). The investigated arealies in the northeastern part of Sirt Basin and extends between latitudes 29°-31°N and longitudes 18° 45'-21° 20`E. The marginal area of the Sirt Basin underwent several tectonic phases owing to the Eurasian-African plates interaction, which is responsible for the development of the structural elements within the basin (Sahell et al., 2010a). During its formation, several subsidence stages of the Basin resulted in many troughs sideways E-W basement deep faults in the early Cretaceous and NW-SE basement faults in late Cretaceous (Burke and Dewey, 1974). A set of platforms separate the troughs. These structural features include the Ajdabiya trough, Jahamah, and Zelten platforms. The thick sedimentary sequence within the Sirt Basin obscures these structural features. Intensive exploration activities for hydrocarbons during the last six decades have been conducted on Sirt Basin. However, the basin's structural setting still needs

much research to be comprehensively understood, particularly the deep-seated faults and shearing structures (Sahell et al., 2010b).

Several authors have conducted gravity and magnetic studies in and around the study area (Essed, 1978; EL-Batroukh and Zentani, 1980; El-Badrawy and Soliman, 2000; Saheel, et al., 2010; Saleem, 2015; Kahoul et al., 2022). The study area is regarded as one of the deepest parts of Sirt Basin rift province (Hallett and Daniel, 2017; Abuhajar and Roohi 2003; Bumby and Guiraud, 2005; Casten and Snopek, 2006; Bosworth et al., 2008; Capitanio, et al., 2009). The investigated area is one of the basin's underexplored regions concerning petroleum potential in Libya (Rusk, 2001; Gong, 2004). The deep subsurface structure and stratigraphy could be significant in distributing possible hydrocarbon accumulations of Sirt Basin. The structural setting of the basin's deep parts is well not known as prospecting activities are focused around the trough, mainly on the shallow margins of the basin and platforms (Ghanush et al., 2014). The complex geological setting, mainly

_____

northern region of Ajdabiya trough, complicates our   understanding of structural trends.

Fig. 1.Simplified geological map of Sirt Basin and study area (After Hallett, 2002).

The current study utilized the magnetic and gravity data to reveal the shear zone structures systems and their depths. This study presents a new element, eliciting a significant number of shears and uses the estimated depths to depict the structural patternof the basement to create a detailed tectonic map of the research area.The chief data sources are Bouguer anomaly and RTP maps of northeastern Sirt Basin. These data are adequate for discerning deep subsurface geological structures and mapping the fractured basement. The initial models for the two profiles traversing the research region were built using the results of the depth estimate methods and the interpreted basement structures, aided by the basement depth in four of the area's boreholes that were used as a critical constraint in the modelling. The research results are not restricted to this region but can be applied to similar regions worldwide.

2. Geological and tectonic setting
Geology
The surface rock units within Sirt Basin are revealed in Figure (1). The rock sequence of the Basin area was accumulated through three rift cycles; pre-rift, syn-rift, and post-rift stages. The rock units range in age from the Cambrian-Ordovician to the Quaternary. In the study area, northeastern Sirt Basin, the Neogene and Pliocene rock units dominate the surface geology (Hallett and Daniel, 2017). The subsurface

stratigraphic column of Sirt Basin is distinguished to pre-, syn-, and post-rift sequences (Fig. 2). Pre- and syn-rift sections are mainly composed of clastics, while the post-rift is mainly consisting of carbonates. The pre-rift sediments were deposited during the Cambrian – Ordovician and consisted of continental conglomerate, sandstone, and shale of the Gargaf Formation (Goudarzi, 1970; 1980). Gargaf Formation is uncon form ably underlain by basement rock and uncon form ably covered by Bahi Formation. Syn-rift stage is characterized by depositing the sediments from late Cretaceous to late Eocene. These sediments are known as basin fill and are mainly of marine origin with variable environments due to Sea level fluctuation, including transgressions and regressions. Their deposition was structurally controlled by NW–SE striking grabens and horsts.The Cretaceous sedimentary rocks uncon form ably overlie Gargaf Formation (Quartizite). The Cretaceous rocks include Bahi sandstone, Waha, and Sirt Shale (Montgomery, 1994; Ghori and Mohammed, 1996; Ambrose, 2000). Tertiary rocks include Hagfa Formation that consists of shale. Hagfa Shale is covered by carbonate, dolomite, shale, and evaporite (Thomas, 1995). The post-rift stage is represented by sandstone of Arida Formation (Oligocene – Miocene). This formation is mainly composed of shallow marine sediments of tidal and supra-tidal environments due to regional regression.
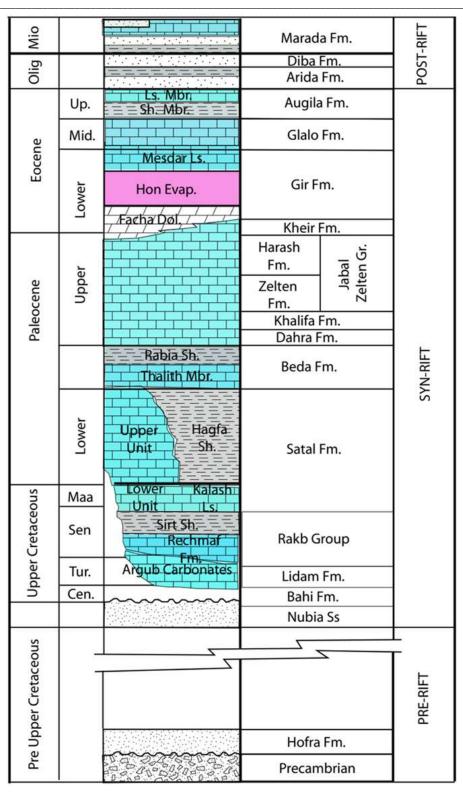
_____

Fig. 2. The stratigraphic column of Sirt Basin (Montgomery, 1994).

Tectonic setting

Throughout the early Paleozoic, thick sedimentary successions were accumulated within the Kalanshiyu trough, northeastern portion of Sirt Basin (Hallett and Daniel, 2017). Paleozoic strata with N-S, E-W, and NE-SWtrends are assumed to be basement rocks in Sirt Basin. Block faulting developed in NW-SE to NNW-SSE zone (Bumby and Guiraud, 2005). Sirt Basin underwent broad arching throughout Hercynian orogeny, which initiated in late Carboniferous and persisted until the early Permian (El-Arnauti et al.,

_____

2008). Pangea was broken up during the Triassic time. The Upper Triassic period was accompanied by a rift phase in Libya and Tunisia (Abadi et al., 2008).

Tectonically, the region was exposed to a series of tectonic activities because of the tectonic interaction between Africa and Eurasia, resulting in several troughs separated by a string of platforms possibly related to major rift stages and reactivated rift faults (Burke and Dewey, 1974). Most basement faults are very steep normal faults with NNW-SSE trend (Gaina et al., 2013). According to de Lamotte et al. (2004), the Tethys sea was originated in late Jurassic and developed during the early Cretaceous. During early Cretaceous, the Sirt Arch collapsed into many grabens with NW-SE and NNW-SSE directions, and Sirt Basin was created from remnant part of the arch (Gumati and Kanes, 1985). Sirt Basin maintained its structural setting until the Late Cretaceous-Paleocene (Saleem, 2015). The basin underwent a reactivation phase in late Cretaceous-early Paleocene period. The Sirt Basin's main structural features have a sedimentation pattern characterized by NW-SE striking structures. The triple connection of the Sarir, Tibesti arms, and Sirt Basin was caused by the rift phase, which started during early Cretaceous, culminated in late Cretaceous, and completed in early Tertiary (Ambrose, 2000). Wennekers et al. (1996) stated that faulting process lead toformation of NW-SE and NNW-SSE faults that affected distribution and positions of platforms and troughs within Sirt Basin. By Oligocene, the last episode of tectonism developed N-S faults, and Ajdabiya trough continued to subside (Hallett and Daniel, 2017).

3.Used materials and analytical techniques

Gravity and reduced to magnetic pole data

Both the Bouguer anomaly map of the investigated area (after the AGOC, 1980 and Libyan Petroleum Institute, LPI, 2001), and RTP map (after the African Magnetic Mapping Project, AMMP), as well as drilled wells data in this area, represent the primary source of the data for revealing the shear zone structures systems and their depths.

Separating and analyzing the potential data

Several separation techniques have been used in the current work to identify the deep shearing of regional trends as follows. The least squares method can potentially produce a high-resolution image of the subsurface. The resulting maps from this technique are beneficial in choosing the particular anomalies to be analyzed and in proving some control in choosing a regional, as this may be indicated by low-order surface fit. As the order increases, residual become smaller and sharper, while the anomaly's relief declines (Nettleton et al., 1960; Skeels, 1967). The horizontal gradient is among the most commonly used

methods to reveal lithological changes with the deformation styles and structural systems over the edges or faults (Zhang et al., 2011). The procedure can be completed by applying pass or rejection filters on Fourier domain data (Sykes and Das, 2000).The tilt derivative is calculated through dividing vertical derivative by sum of horizontal derivatives (Verduzco et al., 2004). It is perfect for tracing anomalies along strike, and this is due to the filter's automated gain control, which equalizes responses from strong and weak magnetic or gravity anomalies. Source edge detection is a technique to locate unexpected lateral modifications in upper crustal rock magnetization from the RTP or gravity data. This method involves locating maxima on a grid of horizontal gradient magnitudes. A database of source edge locations is created from gravity and magnetic gridsusing the Cordell and Grauch (1985) approach.

Depth estimation

The depths and locations of subsurface faults and contacts have been deduced from Bouguer anomaly and RTP maps through the utilization of Euler's deconvolution technique of Thompson (1982) and Reid et al. (1992) using Oasis Montaj V.8.4.2 (Geosoft, 2015). Faulting pictures of each of the gravity and RTP data using solutions with structural index S.I.=0.5 (faults) were carried out. The power spectrum analysis is helpful for potential field data analysis and interpretation since it provides valuable information about the depth of a package of anomalies (anassemblage of causative bodies). In contrast, other conventional depth determination methods concern individual sources (Spector, 1968). Accordingly, spectrum curve is distinguished into two components: the regional component with a high cutoff and the residual component with a low cutoff. This technique was carried out on the gravity and RTP data to determine typical depth levels of the causative sources in the study area using Oasis Montaj V.8.4.2 (Geosoft, 2015).

2D Gravity and magnetic modeling

Using GM-SYS software, the 2D modeling was executed to construct two gravity and magnetic models along two geological profiles (A-A` and B-B`). The profiles were selected to pass by the drilled wells within the investigated area, where the depths of different layers in the two models were compared to depths obtained from drilled wells. The density and magnetic susceptibility values were derived from previous research in this area.

4. Results and discussion
Bouguer anomaly and RTP maps analysis
The Bouguer map of the study area has amplitudes that range from (-24) to (+28) mGal (Fig. 3a). Two lows (L1 and L3) were detected, with E-W trend, three (L2, L4, L5, and L6) with NW-SE trend, and

_____

(L6) with NW-SE trend. High positive anomalies with NW-SE trend that extend from northern to the southeastern parts (H1, H2, H3, H4, and H5) exist on the eastern side. Strong high anomalies (H6), (H7), and (H8), with NW-SE trend extending from northwest to southwest side, were also found in the central part. Another two positive gravity trends extend in NW-SE direction; (H9) in the central part

and (H10) in the southwestern side. The high gravity values with steep gradient suggest that the subsurface structure zones cut crystalline basement rock. The primary gradient reveals juxtaposition of thick Paleozoic-Mesozoicrocks.
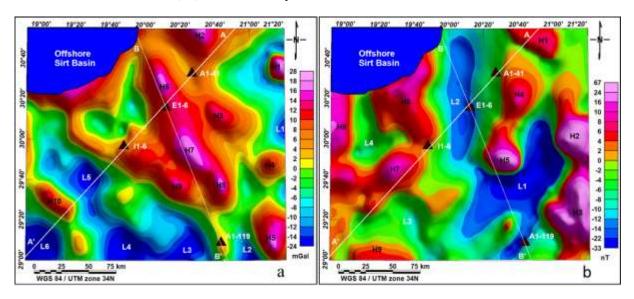

Fig. 3. (a) The Bouguer anomaly and (b) RTP maps of the in vestigated area. Letters show gravity and magnetic anomalies. Triangles show sites of four wells used for 2D modelling along profiles A-A' and B-B'.

The interpreted subsurface fault system and shear zones deduced from the study area's gravity, and RTP maps are shown in Figures (4 and 5).
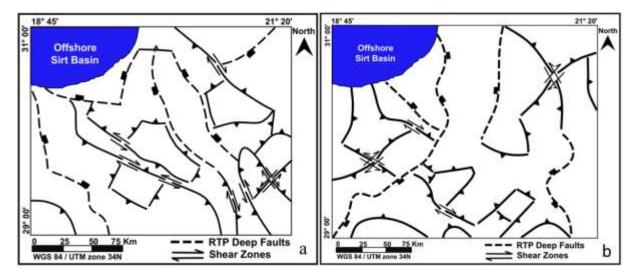

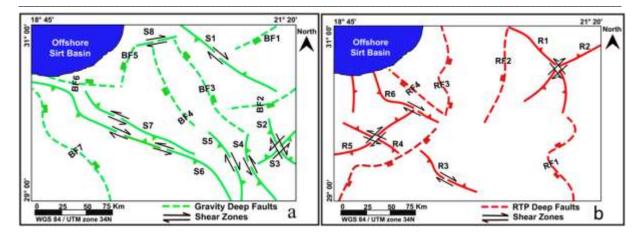Fig. 4. Fault system deduced from (a) Bouguer and (b) RTP maps.

Fig. 5. Deep fault system and shear zones deduced from (a) Bouguer and (b) RTP maps.

Separating and analyzing the potential data

Least squares method

The least squares method was performed on gravity and RTP data to estimate residual gravity and magnetic components. The calculated correlation coefficients between the different successive residual gravity maps are r1= 0.824277, r2= 0.881497, and r3= 0.926437. Using this criterion, the residual gravity field in this area could thus exclusively be denoted by a third-order surface (Fig. 6a). For magnetic data, correlation coefficients among successive residuals were calculated as r1=. 0.884373, r2= 0.944597 and r3= 0.967763. Thus, the residual magnetic field might be denoted by a third-order surface (Fig. 6b).
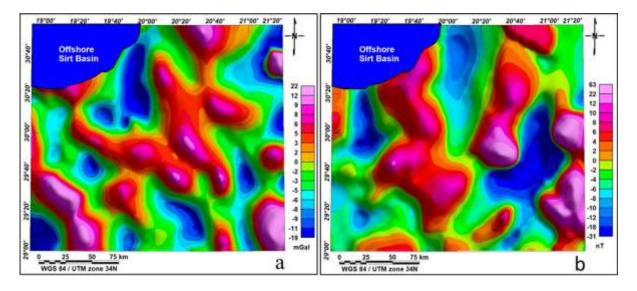

Fig. 6. (a) Residual gravity and (b) residual magnetic maps generated using the least squares method.

Horizontal gradient

This technique was carried out to both gravity and RTP data. The gravity anomalies were elucidated by the horizontal gravity gradient across the entire research area (Fig. 7a). The northern, central, western, and southern regions exhibit many strong horizontal gradient anomalies with NW-SE trends. The E-W and N-S trends on the eastern side were curtailed. The horizontal gradient filter of the RTP data shows strong gradients with N-S to NW-SE trends on the eastern and northern sides (Fig. 7b). Also, the northwestern and southwestern regions have high gradients in the N-S and NW-SE trends.
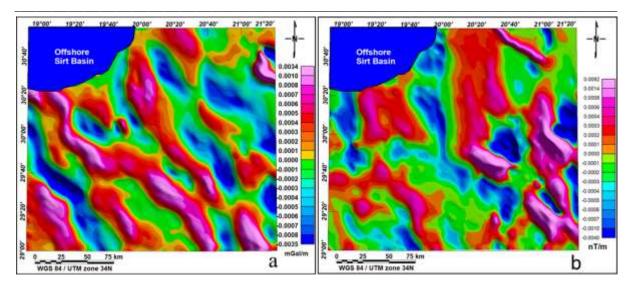
Fig. 7.The horizontal gradient of the (a) gravity and (b) RTP data.

Tilt derivative filter

The tilt derivative filter (TDR) is applied to reveal edges of subsurface blocks and the orientations of deep-seated structures or faults. Figures (8a and 8b) show the results from TDR maps of gravity and RTP data, respectively, with zero contour lines (black line) outlining edges of subsurface causative sources. Figure (8a) reveals that the gravity-causative bodies have N-S trend on the eastern side and northern part of the map. In contrast, the causative bodies strike in the NW-SE direction in the central, western, and southern parts. On the other hand, Figure (8b) reveals causative bodies with N-S and NNE-SSW trends in the map's eastern half, while the western half reveals causative bodies with N-S, NE-SW, and E-W trends.
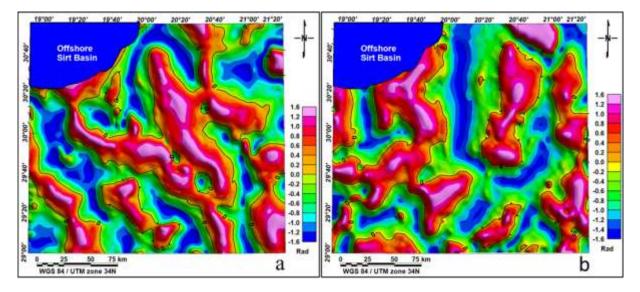

Fig. 8. Tilt derivative of (a) gravity and (b) magnetic data. The zero contours are plotted in solid lines representing the boundaries of the causative bodies.

Source edge detection

The technique was conducted on the Bouguer and RTP maps to deduce lateral variations in the rock magnetization and gravitation. Symbols shown depict the locations and gradient directions of probable field anomalies on gravity and magnetic grids (Fig. 9a and b).
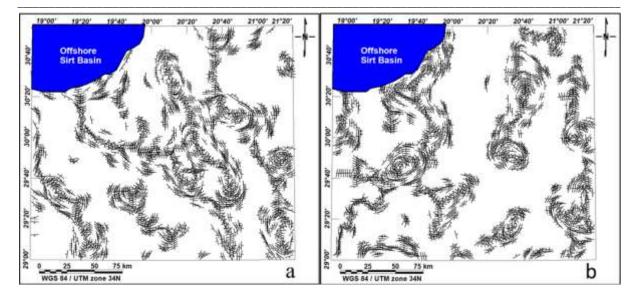
Fig. 9.The source edge detection of (a) the gravity and (b) magnetic data.

Depth estimation

Euler deconvolution

The Euler technique with a S.I= 0.5 was conducted to reveal the fault picture of the gravity data. The total solution of the gravity reveals depth ranging between 0.39 and 4.55 km with a mean depth of 1.78 km (Fig. 10a). It demonstrates excellent clustering in both linear and curved directions, with a group of faults having main trends of NW-SE, E-W, N-S, and NE-

SW. On other hand, the Euler total solution of the magnetic data with the same SI, shows that the depth ranges between 0.40 and 5.25 km with a mean depth of 1.64 km (Fig. 10b). The magnetic plots show that several regional faults with NE- SW, NW-SE, and N-S directions dissected the study area.
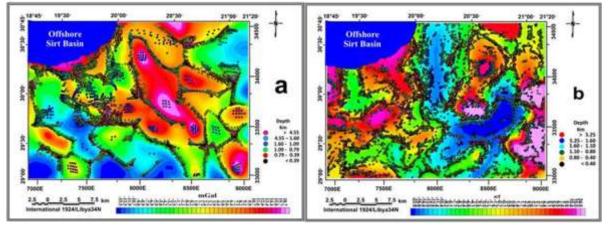

Fig. 10. Euler deconvolution solutions of the (a)gravity and (b) magnetic data.

The plot solution for both gravity and RTP data was resolved and traced to throw more light on the subsurface faults as well as to give more accurate pictures of faults (Fig. 11) that affect the study area at successive depths every 0.25 km as follows:

i. Faulting picture at depth interval 0.01 - 0.39 km:
    The plot solutions of gravity data shown in Figure (11a) reveal the presence of shallow faults scattered

throughout the area. The magnetic solution (Fig. 11b) shows the first appearance of fault directions, especially in the northern, southern, and eastern regions.

ii. Faulting picture at depth interval 0.40 - 0.79 km:
    Both gravity and magnetic solutions are shown in Figures (11c and 11d), respectively, and are characterized by high increases and clustering in their

numbers and distribution. At this depth interval, the deep shear zones begin to monitor, which reveals that the shear zones have a deeper extent throughout the region.

iii. Faulting picture at depth interval 0.80 - 1.09 km:
The solution numbers of gravity data at this level (Fig. 11e) decrease while the plot solution of RTP data (Fig. 11f) shows a slight decrease. At this depth interval, the faults became more apparent and visible as they engulfed some of them, especially in the northeastern and western sides and the southeastern and central parts.

iv. Faulting picture at depth interval 1.10 - 1.60 km:The number of gravity solutions at this level (Fig. 11g) still decreased, with the emergence of some faults that disappeared in the previous depth interval. The plot solution of magnetic data (Fig. 11h) slightly

decrease, and the faults became more apparent and visible as they engulfed some of them, especially on the eastern and western sides.

v. Faulting picture at a depth range 1.61 - 4.55 km:
The gravity solutions number shown in Figure (11i) is still decreasing, and some faults have disappeared, as in northern central and western regions. Magnetic solution (Fig. 11j) retained the large shear zones that affected the area and remained clearer and conspicuous, especially in the central, eastern, north western, and southern parts.

It is evident from resolving and tracking the plot solution of gravity and RTP data that the shear zones and faults affecting the study area, which can be tracked at successive depths, are similar to those previously inferred and shown in Figures (4 and 5).
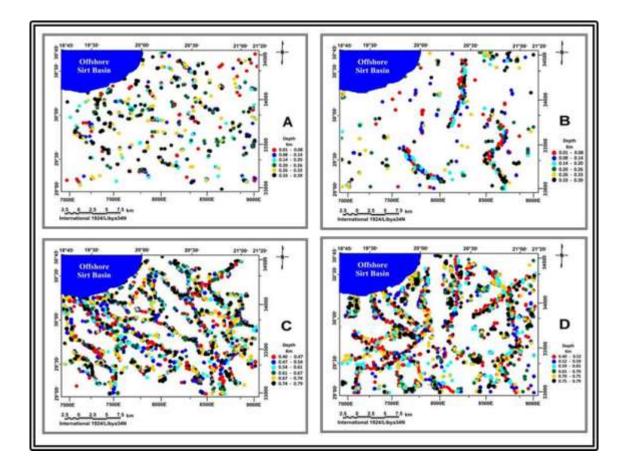

Fig. 11. 3D Euler deconvolution solutions (A,C,E,G, and I) of gravity data, and (B,D,E,H, and J) of magnetic data at different depths.
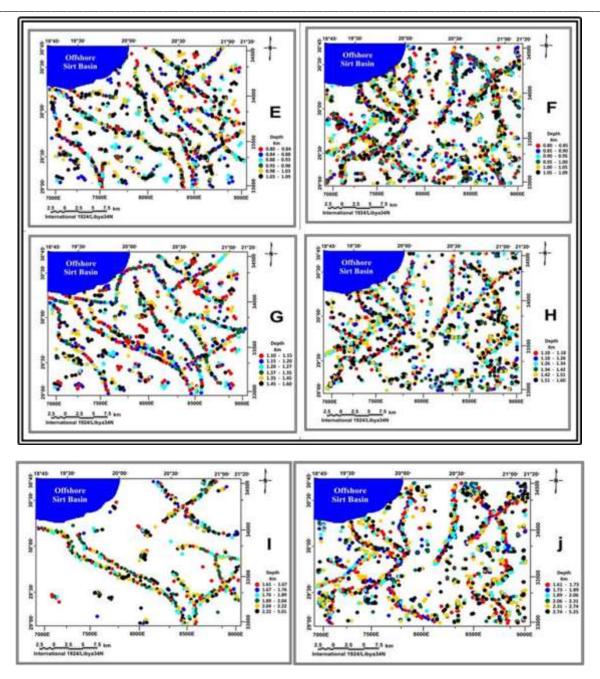
Fig. 11. (Continued).

Power spectrum analysis

In the current study, the gravity and RTP maps underwent the Fourier transformation using Geosoft software (V.8.4.2) to compute the energy spectrum as a power spectrum curve. Figures (12a and b) show the estimated depth to deep and shallow causative sources deduced from the gravity and RTP data. As seen on the graph, the deep depth is 4.5 km for gravity and 5.11 km for RTP data, which almost agrees with the greatest basement depth. The 3.5 km lies within the depth range of basement, whereas the last two values (1.22 km and 1.34 km) correspond to the shallow sources. The abovementioned magnetic and gravity data analysis and the information obtained from the applied techniques agree well with the basement depths. These depths match well with the depths obtained from drilled wells in the area, such as wells A1-41, A1-119 and E1-6, which reach granite rocks at depths 4.604, 4.179, 4146, and 1.200 km, respectively.
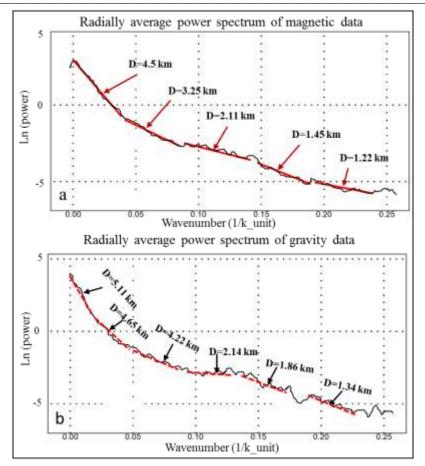
Fig. 12. Radially averaged power spectrum analysis of (a) gravity and (b) magnetic data.

2D Gravity and magnetic modelling

Two gravity and magnetic models were generated using GM-SYS software. The first 2D model was constructed along profile (A-A'), that extend NE-SW for 210 km and passes by wells No. I1-6, E1-6, and A1-41 (Fig. 13a). The resulting faults in this 2D model correspond to the faults identified in the north western part of the area, which were deduced from the tectonic and Euler maps as presented in figures (4, 5, and 10). The second 2D model was built along profile (B-B`), extending NW-SE for 195 km; it passes by wells No. E1-6 and A1-118 (Fig. 13 b). The results of this 2D forward modelling clarify the local igneous intrusion (maybasic) during the Cenozoic. The faults are also clarified by Euler's solutions and tectonic maps as presented in figures (4, 5, and 11).

Tectonics of the investigated area

A tectonic map for the northeastern portion of Sirt Basin was constructed based on the fault system deduced from both gravity and magnetic maps (Figs. 4 and 5) and the Euler resolved solutions at sequential depths (Fig. 11). This map (Fig. 14) reveals deep-seated faults and shear zones controlling the structural

setting in the subsurface of the investigated area. From close examination of this map, it could be concluded that:

i. The Bouguer anomaly map shows that eight shear zones (S1-S8) with different trends could be detected. Shear (S1) extends NW-SE at the north eastern side, shears (S2-S5) are recorded at the south eastern side with two of them crosscutting the other two. Shears 6 and 7 extend NW-SE while the remaining S8 extends E-W along the northern part of the study area. Most of these shears (S1), (S2), (S5), (upper portion of S6), and (S8) are related to dextral strike-slip (right-lateral) movement. The shears (S3), (S4), (lower portion of S6), and (S7) are related to sinistral strike-slip (left-lateral) movement (Fig. 5a).

ii. Seven large deep faults can be inferred from the Bouguer map; (BF1) and (BF2) with NE-SW trend, and (BF3) and (BF4) with NW-SE trend. The western side was affected by three deep faults; (BF5), (BF6), and (BF7), with N-S, E-W, and NW-SE trends, respectively (Fig. 5a).
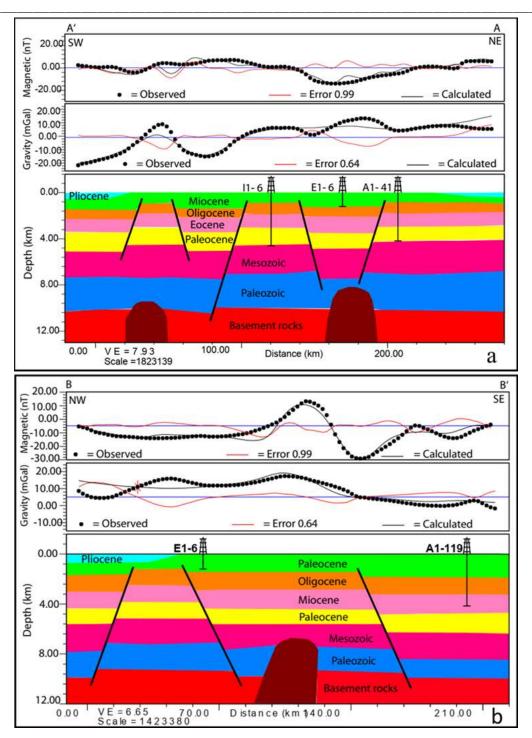
Fig. 13. 2D Forward gravity and magnetic modelling across (a) profiles A-A′ and (b) B-B′.

iii. All the subsurface structures, such as shears or deep faults with NW-SE trend were formed due to movements along the Mediterranean Sea (Tethyan). The Mediterranean Sea trend is considered a major predominant trend across Sirt Basin. This trend is related to the early Cretaceous rift phases and crustal extension period. Moody (1973) explained this trend as a simple compressional fold-thrust trend that originated due to compressive stress in the north-south direction. The structures with NE-SW and N-S trends inherited from Pan-African and late Palaeozoicorogenies were active during early Cretaceous and culminated during the Tertiary. They were related to reverse faulting started in late Cretaceous during the continental collision between Africa and Eurasia (McKenzie, 1970). These old basement structural elements have been reactivated during Phanerozoic Eon (Bumby and Guiraud,

2005). Also, the structures with E-W trend may have started in early Cretaceous rift due to the NS extension along the Neo-Tethysrim. This conclusion agrees with Dercourt et al. (1986); Anketell (1996); Guiraud and Bosworth (1998); Burwood et al. (2003); Elakkari (2005); El Arnauti et al. (2008); Saheel et al. (2010); Ghanush et al. (2014); Abdunaser and McCaffrey(2015) and Ghanush (2019).

iv. The RTP map shows six shear zones (Fig. 5b) where the shear (R1) with NW-SE trend is intersected by shear (R2) with NE-SW trend on the northeastern side. The shear (R3) with NW-SE trend lies in the southern side. Shear (R4) with NW-SE trend is cut by shear (R5) with NE-SW trend on the western side. The last shear (R6) with NW-SE trend is located on the northwestern side.

v. The movements of the Arabian and African plates and the incipient of the East African Rift system, which initiated in the Precambrian and rejuvenated many times during the Pre-Carboniferous Herecynian, late Cretaceous Laramid, and late Tertiary Alpine orogenies

resulted in the development of these wrench zones. Thus, these tectonic events resulted in a dextral strike-slip reactivation of the Megashear System of North Africa. Also, a sinistraltranstensional reactivation of the northwest striking faults arose the dextral reactivation of the North African Megashear System.

vi. Four large deep faults (RF1 to RF4) could be traced from the RTP map and are distributed throughout the area with NS, NE-SW, and NW-SE directions (Fig. 5b). All these faults are thought to have been caused by the northward drift of the African plate and its collision with Eurasian plate. Their origin is also related to the early Tertiary. This view matches (Roohi, 1996a and 1996b; Hallett and Daniel, 2017; Harding, 1984).

Therefore, we may state that some shear zones that are inferred from both the gravity and RTP maps (S1&R1) and (S7&R6) coincide, with a slight deviation in the coordinates. It is therefore possible to collectively say that the present area may comprise 11 shears as deduced from the Bouguer and RTP maps.
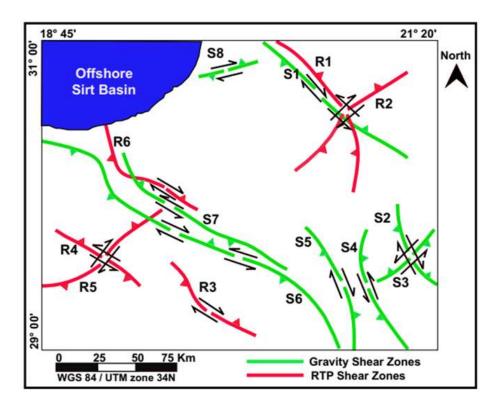

Fig. 14. Final interpreted shear zones of the study area.

5. Conclusions

The Bouguer gravity and RTP magnetic maps have been proven to be adequate and valuable in elicitation of the deep structures and shear zones in

north east Sirt Basin. The potential field gravity and magnetic data are available with a considerable resolution and valid for eliciting regional tectonic

features. The development of the deep structures and shear zones beneath the Sirt Basin is mainly controlled by the tectonic interaction between Africa and Laurasia. Eleven major shear zones that have not been revealed before could be traced in the study area. Seven shear sets (S1 to S7) were deduced from Bouguer map and six (R1 to R6) from the RTP map. It is noticed that some of these shear zones intersect each other, such as (S2 with S3) and (R1 with R2), (R4 with R5). These intersection points weakened the Earth's crust in this area, which in turn makes it tectonically unstable. Also, (S1 and S7) that are traced from the gravity map coincide with (R1 and R6), which are traced from the RTP map. These subsurface tectonic structures, shears, or faults affecting this area were monitored through interpreted fault systems and the Euler deconvolution technique. These wrench zones are expected to be due to movements of the Arabian and African plates and also the resulting East African Rift system started in the Precambrian time and rejuvenated during the Herecynian (Pre-Carboniferous), Laramid (Late-Cretaceous) and Alpine (Late-Tertiary) orogenies. This led reactivating the Megashear System of North Africa in a dextral strike-slip pattern. Sinistral transtensional reactivation of northwest striking faults arose from the dextral reactivation of the Megashear System of North Africa.

6. Acknowledgments

References

Abadi AM, van Wees JD, van Dijk PM, Cloetingh SA (2008) Tectonics and subsidence evolution of the Sirt Basin, Libya. American Association of Petroleum Geologists Bulletin, 92, 8, 993–1027. DOI: 10.1306/03310806070

Abdunaser KM, McCaffrey KJ (2015) Tectonic history and structural development of the Zallah-Dur al Abd Sub-basin, western Sirt Basin, Libya. Journal of Structural Geology, 73,33-48.

Abuhajar MI, Roohi M (2003) Giant Fields in the Sirt Basin, Libya: 1st EAGE North African/Mediterranean Petroleum & Geosciences Conference & Exhibition, European Association of Geoscientists and Engineers, 255–279. https://doi.org /https: //doi.org/10.3997/2214-4609-pdb.8.S025.

Ambrose G (2000) The geology and hydrocarbon habitat of the Sarir Sandstone, SE Sirt Basin, Libya. Journal of Petroleum Geology, 23, 165-191.

Anketell JM (1996) Structural history of the Sirt Basin and its relationship to the Sabrata Basin and Cyrenaica Platform, northern Libya, The Geology of the Sirt basin, pp.57-89.

Bosworth W, El-Hawat AS, Helgeson DE, Burke K (2008) Cyrenaica shock absorber and associated inversion strain shadow in the collision zone of northeast Africa, Geology, 36(9), 695–698.

Bumby AJ, Guiraud R (2005) The geodynamic setting of the Phanerozoic basins of Africa. Journal of African Earth Sciences, 43(1-3), 1-12.

Burke KCA, Dewey JF (1974) Two plates in Africa during the Cretaceous? Nature, 249, 313–316.

Burwood R, Redfern J, Cope M (2003) Geochemical evaluation of East Sirte Basin, Libya petroleum systems and oil provenance. Geological Society of London Special Publication, 207, 203–240. https ://doi.org/10.1144/ GSL.SP.2003.207.11.

Capitanio FA, Faccenna C, Funiciello R (2009) The opening of Sirte basin: Result of slab avalanching. Earth and Planetary Science Letters, 285, 210–216.

Casten U, Snopek K (2006) Gravity modelling of the Hellenic subduction zone a regional study, Tectonophysics, 417, 183–200.

Cordell L, Grauch VJS (1985) Mapping basement magnetization zones from aeromagnetic data in the San Juan Basin, New Mexico. In The utility of regional gravity and magnetic anomaly maps, Society of Exploration Geophysicists, 181-197.

de Lamotte DF, Crespo-Blanc A, Saint-Bézar B, Comas M, Fernandez M, Zeyen H, Zizi M (2004) Transect I: Iberian Meseta–Guadalquivir Basin– Betic Cordillera–Alboran Sea–Rif–Moroccan Meseta–High Atlas–Sahara Platform. The Transmed Atlas: The Mediterranean Region from Crust to Mantle, Springer, Berlin, 141.

Dercourt J, Zonenshain LP, Ricou LE, Kazmin VG, Le Pichon X, Knipper AL, Grandjacquet C, Sbortshikov IM, Geyssant J, Lepvrier C, Pechersky DH, Boulin J, Sibuet JC, Savostin LA, Sorokhtin O, Westphal M, Bazhenov ML, Lauer JP, Biju-Duval B (1986) Geological evolution of the Tethys belt from the Atlantic to the Pamirs since the Lias. Tectonophysics, 123: 241-315.

Elakkari TS (2005) Structural configuration of the Sirt Basin, MSc. Thesis, International Institute for Geo-Information Science and Earth Observation Enschede, The Netherlands, 69p.

El-Arnauti A, Shelmani MA, Lawrence SR, Mansouri A, Sengör AMC, Soulsby A, Hassan M (2008) Structural styles in N.E. Libya. Sedimentary Basins of Libya, Third Symposium, Geology of East Libya, 4, 153-178.

El-Badrawy HT, Soliman MR (2000) Continuation of geophysical data in delineating the subsurface tectonic structures of Sirt Basin, Libya. 5th International Conference on the Geology of the Arab World, Cairo University, 683-698.

El-Batroukh SI, Zentani AS (1980) Gravity interpretation of Raguba field, Sirte basin, Libya. Geophysics, 45, 1153-1163.

Essed AS (1978) A reconnaissance Bouguer gravity map of Libya, M.Sc. thesis, Purdue University United States.

Gaina C, Torsvik TH, van Hinsbergen DJJ, Medvedev S, Werner SC, Labails C (2013) The African Plate: A history of oceanic crust accretion and subduction since the Jurassic, Tectonophysics, 604, 4– 25.

Geosoft reference manual (2015) software for Earth Sciences Geosoft INC., Toronto, Canada.

Ghanush H (2019) Structure of the Ajdabiya Trough, NE Sirt Basin, Libya, Derived from Gravity and Magnetic Data. International Journal of Science and Research, 8:1289–1304.

Ghanoush H, Imber J, McCaffrey K (2014) Cenozoic Subsidence and Lithospheric Stretching Deformation of the Ajdabiya Trough Area, Northeast Sirt Basin, Libya. In American Association of Petroleum Geologists Annual Convention and Exhibition, Houston, Texas.

Ghori KAR, Mohammed RA (1996) The application of petroleum generation modelling to the eastern Sirt Basin, Libya, in Salem MJ, El-Hawat AS, Sbeta AM (eds.), The geology of Sirt Basin: Amsterdam, Elsevier, v. II, pp 529–540.

Gong J (2004) Framework for the exploration of Libya: an illustrated summary. American Association of Petroleum Geologists Search Discovery Article 10061.

Goudarzi GH (1970) Geology and mineral resources of Libya: a reconnaissance. United States Geological Survey. Professional Paper no. 660, Washington, p 104.

Goudarzi GH (1980) Structure—Libya, in Salem MS, Busrewil MT (eds.), The Geology of Libya: London, Academic Press, v. 3, pp 879–892.

Guiraud R, Bosworth W (1998) Senonian basin inversion and rejuvenation of rifting in Africa and Arabia: synthesis and implications to plate-scale tectonics. Tectonophysics, 282:39–82. https ://doi.org /10.1016/ S0040 -1951 (97) 00212 -6.

Gumati YD, Kanes WH (1985) Early Tertiary subsidence and sedimentary facies northern Sirt Basin, Libya. American Association of Petroleum Geologists Bulletin, 69:39–52. https://doi.org/10.1306/AD461B83-16F7-11D7-8645000102C1865D.

Hallett D (2002) Petroleum geology of Libya. Elsevier, Dordrecht, p 297.

Hallett D, Daniel CL (2017) Petroleum geology of Libya. Elsevier, New York.

Harding TP (1984) Graben hydrocarbon occurrences and structural style. American Association of Petroleum Geologists Bulletin, 68(3), 333-362.

Kahoul S, Sidek A, Eshanibli A, Trepil F, Jaafar MZB, Hassan M, Ghanoush H, Dugdug L (2022) Identifying fault system and basement depth using aeromagnetic data beneath the jahamah platform, NE Sirt Basin, Libya. Acta Geodynamicaet Geomaterialia, 19 (2), 155–166. DOI: 10.13168/AGG.2022.0005.

McKenzie DP (1970) The plate tectonics of the Mediterranean region, Nature, 226, 239-243.

Moody JD (1973) Petroleum exploration aspects of wrench fault tectonics, American Association of Petroleum Geologists Bulletin, 57 (3), 449 – 477.

Montgomery S (1994) Sirte Basin, North-Central Libya, prospects for the future: Petroleum Frontiers, Petroleum Information Corporation, 11, no. 1, 94 p.

Nettleton LL, LaCoste LJB, Harrison JC (1960) Tests of an airborne gravity meter: Geophysics, 25, 181-202.

Reid AB, Allsop JM, Granser H, Millett AT, Somerton IW (1990) Magnetic interpretation in three dimensions using Euler deconvolution. Geophysics, 55(1), 80-91.

Roohi M (1996a) Geology of Sirt Basin, First symposium of the sedimentary Basins of Libya, 2, 323-336.

Roohi M (1996b) Geological history and hydrocarbon migration pattern of the central AzZahrah-Al Hufrah Platform.First Symposium on the Sedimentary Basins of Libya, *in* Salem MJ, El-Hawat AS, Sbeta AM (eds.), Geology of the Sirt Basin, vol. 2. Elsevier, Amsterdam, 435-454.

Rusk DC (2001) Petroleum potential of the under-explored basin Centers Libya—a 21st-century challenge. American Association of Petroleum Geologists Bulletin, 83, 429–452.

Saheel AS, Samsudin AR, Hamzah U (2010a) Interpretation of the gravity and magnetic anomalies of the ajdabiya trough in the sirt basin, Libya.European journal of scientific research, 43 (3), 316-330.

Saheel AS, Samsudin AR, Hamzah U (2010b) Regional geological and tectonic structures of the Sirt Basin from potential field data. American Journal of Scientific and Industrial Research, 1, 3, 448–462. DOI: 10.5251 /ajsir. 2010.1.3.448.462.

Saleem MAA (2015) Tectonic evolution and structural analysis of south-western Sirte Basin, Central Libya.PhD. Thesis, University of Birmingham.

Skeels DC (1967) What is the residual gravity, Geophysics, 32, 872–876.

Spector A (1968) Spectral analysis of aeromagnetic maps.Ph. D. Thesis, Department of Physics, University of Toronto, Canada.

Sykes MP, Das UC (2000) Directional filtering for linear feature enhancement in geophysical maps. Society of Exploration Geophysicists, 65(6), 1758.https: //doi.org /10.1190/1.1444860.

Thomas D (1995) Exploration limited since 70s in Libya's Sirte basin. Oil and Gas Journal, 93(11), 99-104.

Thompson DT (1982) EULDPH: a new technique for making computer-assisted depth estimates from magnetic data. Geophysics, 47, 31–37.

_____

Verduzco B, Fairhead JD, Green CM, Mackenzie C (2004) New insights into magnetic derivatives for structural mapping. The leading edge, 23(2), 116-119.

Wennekers, J.H.N., Wallace, F.K. and Abugares, Y.I., 1996. The geology and hydrocarbons of the Sirt Basin: a synopsis. The geology of the Sirt Basin: Amsterdam, Elsevier, 1, 3-56.

Zhang HL, Liu TY, Yang YS (2011) Calculation of gravity and magnetic source boundaries based on anisotropy normalized variance. Chinese Journal of Geophysics, 54(4), 560-567.

استنتاج التراكيب القصية التكتونية في الجزء الشمالي الشرقي من حوض سرت بليبيا كما تم استنباطها من بيانات مجال الجهد

حسين توفيق البدراوي، ومصطفى ناجي، وحامد عبدالحميد الرفاعي

قسم الجيولوجيا، كلية العلوم، جامعة كفر الشيخ، مصر

تهدف هذه الدراسة إلى استنتاج نطاقات القص تحت السطحية التي أثرت في الجزء الشمالي الشرقي من منطقة حوض سرت، والتي تعتبر من أهم المناطق المنتجة للنفط، وتأثيرها على مناطق مماثلة حول العالم. لتحقيق هذا الهدف، تم تطبيق العديد من التقنيات الجيوفيزيقية على بيانات الجاذبية وبيانات المغناطيسية الأرضية المحولة الى القطب المغناطيسي الشمالي. تشمل هذه التقنيات المربعات الدنيا، والمشتقة المائلة، والتدرج الأفقي، وتحديد حافة المصدر. بالإضافة إلى ذلك، تم إجراء تحليل أويلر وتحليل طيف القوى بهدف تصوير الصدوع المتواجدة على الأعماق المتتالية العميقة. وكذلك تم إنشاء نماذج جاذبية ومغناطيسية ثنائية الأبعاد على طول قطاعين بدلالة أربعة آبار محفورة في منطقة الدراسة. وقد تم الكشف عن إحدى عشرة مجموعة جديدة من نطاقات القص تحت السطحية والتي لم يتم استنتاجها من قبل وذلك من خلال الخريطة التكتونية المستنتجة للصدوع في منطقة الدراسة، حيث أن معظم هذه الصدوع من النوع المضربي يساري الحركة (سنيسترال) وبعضها يميني الحركة (ديكسترال). كما تم تتبع هذه النطاقات القصية على ستة مستويات متتالية للعمق لمعرفة ما إذا كانت سطحية أم عميقة. حيث تم الكشف عن سبع مجموعات نطاقات قصية من بيانات الجاذبية وستة أخرى من بيانات المغناطيسية. وقد وجد أن مجموعتين من النطاقات القصية المستنتجة من الجاذبية تتطابق مع مجموعتين من النطاقات القصية المستنتجة من خريطة المغناطيسية. تتقاطع بعض هذه النطاقات القصية مع بعضها البعض، وقد أدت نقاط التقاطع هذه إلى إضعاف قشرة الأرض والتي بدورها تصبح غير مستقرة من الناحية التكتونية في هذه المنطقة. من المتوقع أن تكون هذه النطاقات القصية ناتجة عن الحركات التكتونية للصفائح العربية والأفريقية بالإضافة إلى خسف شرق إفريقيا والتي أدت إلى إعادة تنشيط النظام القصي العظيم في شمال إفريقيا في نمط انزلاق مضربي يميني الحركة. بينما يعزى إعادة التنشيط يساري الحركة للصدوع ذات الاتجاه شمال غرب إلى إعادة التنشيط يميني الحركة للنظام القصي العظيم في شمال إفريقيا.

_____